CHARACTERIZATION OF SODIUM AND FLUORIDE PENETRATION INTO CARBON CATHODES BY IMAGE ANALYSIS AND SEM-EDS TECHNIQUES

Yuanling Gao, Jilai Xue, Jun Zhu, Kexin Jiao, Gangqiang Jiang
School of Metallurgical and Ecological Engineering, University of Science and Technology Beijing
Xueyuan Road 30, 100083 Beijing, China

Keywords: Cathode material, Pore distribution, Image analysis, Sodium and fluoride penetration

Abstract

The porous structure of carbon cathodes is materials dependent, which can be related to sodium and fluoride penetration during aluminum electrolysis. This work is aimed at developing a better digital method for characterization of the pores and the penetration resistance of the cathode products. The profiles of penetrated Na, F, Al versus penetration depth in the cathode samples after aluminum electrolysis were obtained using SEM-EDS analysis. The internal porosity, pore size distribution, pore shape and orientation and pore connectivity were also characterized by image analysis. It is found that the graphitization, total and partial porosity, pore orientation and connectivity can contribute to the sodium and fluoride penetration into the carbon cathodes. The penetration behaviors varied with change in cathode materials (from semi-graphitic, full graphitic to graphitized carbons).

Introduction

Numerous publications have dealt with improving cathode properties and performance in aluminum reduction cells. One of important reasons to use more graphitic and graphitized cathode materials is to have better resistance to sodium and fluoride attack. This can lead to a longer cell service life while a higher cost for cathode materials.

The carbon or graphite cathodes have a porous material structure, which is developed in both the cathode forming and baking stages [1]. Porosity and density are important properties for cathode quality [2]. Sodium and fluoride penetration in aluminum electrolysis have received considerable attention for various carbon, graphite and composite materials [3-4], where higher graphitization is usually recognized for better resistance to sodium attack. In recent years, image analysis methods have been used to study carbon anode porosity [5-9], but there is so far no open literature reporting its application in studying the cathode pores.

The aim of this work is to find a computer aided, statistical approach characterizing both pore parameters and sodium/fluoride penetration properties. In this paper, the samples tested were taken from various industrial cathode products and image analysis and SEM-EDS methods were applied together before and after aluminum electrolysis. The pore parameters obtained were interpreted in association with the results from sodium and fluoride penetration studies.

Experimental

Preparation of Samples

Table I shows some selected physical properties of the cathode samples used in this investigation. These were directly taken from various industrial cathode products of semi-graphitic (HC35), full graphitic (HC100), and graphitized carbons (SMH). All cathode samples were made in cylindrical form and their apparent density, open porosity and compressive strength were measured according to the relevant industrial standards.

Table I. Physical Properties of Cathode Samples

Sample	Apparent Density (g/cm^3)	Open Porosity (%)	Compressive Strength (MPa)
HC35	1.57	14.04	27.84
HC100	1.61	18.12	33.06
SMH	1.54	22.27	19.17

For further optical microscopy inspection, the cylindrical cathode samples were sliced along their longitudinal axis, and the cutting surface on the cross-section of each segment was ground and polished according to an ASTM standard [10] modified with no polishing agent used.

Image Analysis Method

Figure 1 is a flowchart illustrating the image acquiring and processing procedures used for the sliced cathode samples. The microscopy photographs of the samples were obtained by a standard polarization microscope (Leica, DMRX). The image analysis was performed using Image J software (a public domain, Java-based image processing program developed at the National Institute of Health). Image J was designed with an open architecture that provides extensibility via Java plugins and recordable macros.

The digital image processing method was able to eliminate some miscellaneous, irrelevant details and enhance the total image quality. The skeletonization obtained by an image thinning operation was used to reflect the pore connectivity within the carbon cathode materials. The 2D data at each segment obtained from the image analysis were applied to statistically express some essential characteristics of the cathode materials.

The total porosity of each cathode sample was determined from the average porosity data of five arbitrary regions (768×582) on one segment. The value of pore size distribution (PSD) is the sum of the areas of pores in a certain interval of pore diameter, where the diameter is a mean length of lines crossing the pore centroid per 5 degree in angle. Pore shape was described by the aspect ratio of the longest diameter to the shortest diameter crossing the pore centroid. Pore orientation and connectivity were also studied for comparison of the three cathode materials.
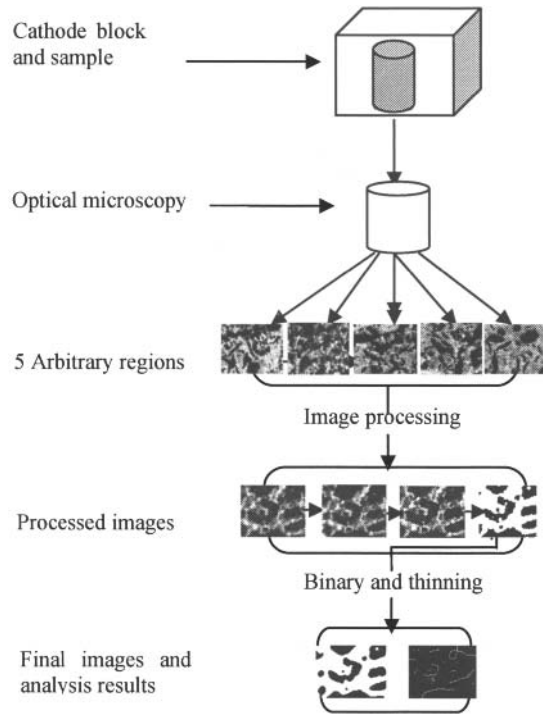
Cathode block and sample

Optical microscopy

5 Arbitrary regions

Image processing

Processed images

Binary and thinning

Final images and analysis results

Figure 1. Image acquiring and processing procedures for analyzing cathode samples

Sodium/Fluoride Penetration and SEM-EDS Examination

Sodium and fluoride penetration tests during aluminum electrolysis were carried out in a laboratory cell, as described previously [3, 11], at a cathode current density of 0.5 $A \cdot cm^{-2}$ and temperature of 960 C. The cylindrical cathode sample (dia 15x60 mm) was immersed 2 mm in the cryolitic melt (cryolite ratio = 4) containing 5 wt.% Al_2O_3 and 5 wt.% CaF_2. Both the sodium generated during aluminum electrolysis and the fluorides (NaF, Na_3AlF_6, etc) from the bath were penetrated into the cathode body along its axis direction.

After the electrolysis experiment for 3 hours, the cathode sample was cut open along the longitudinal axis, and the penetration depth and the amount of penetrated sodium and fluoride were determined by SEM-EDS analysis with scanning time of 90 seconds crossing the area for each 1 mm along the axis direction. The penetrated metals and fluorine in the cathode samples were then expressed in term of the relative percentage of F, Na, Al, Ca and C against the penetration depth.

Results and Discussion

Pore Distribution

Table II presents the resulting data from characterization of the pores, where the 2D data could reflect the relevant 3D parameters of the pores. The specific surface area of pore can also be

calculated from the perimeter of the area of the pore according to Saltykov equation [12]:

$$S = 4 \, L_p/\pi A_p \qquad (1)$$

where L_p is the mean perimeter of pores on the cross-section surface and A_p is the mean area of pores.

HC35 cathode sample exhibits a higher total porosity but lower number of pores than HC100 sample, while SMH has the highest total porosity (25.48%) among the three cathode samples. For the partial porosity with D_{mean} below 600 μm (%), the graphitized cathode sample is also the highest one (15.27%), followed by HC100 and HC35. The partial porosity mainly is the reflection on the inner micropores for the cathode materials, which could be related to some surface properties, such as capillary force, wetting angle, etc.

Table II. Statistical Results of Image Analysis on the Pores in Cathode Samples

Samples	HC35	HC100	SMH
Total Porosity (%)	21.05	15.35	25.48
Partial Porosity with D_{mean} below 600 μm (%)	7.31	13.08	15.27
Number of Pores	230	488	438
Average Pore Diameter (μm)	186.61	135.97	182.31
Specific Surface Area of Pore ($\mu m^2/\mu m^3$)	0.017	0.029	0.023

Figure 2 further reveals the details of the fraction difference of pores in terms of the pore size distribution (PSD) among the three cathode materials. The major fractions of the pores in HC35 and SMH cathode samples are the meso pores between 300 μm and 900 μm in mean diameter, while a large part of fractions in HC100 samples are the micropores bellow 300 μm. HC35 cathode sample has more fractions in the macropores (>900 μm) than HC100 and SMH samples.
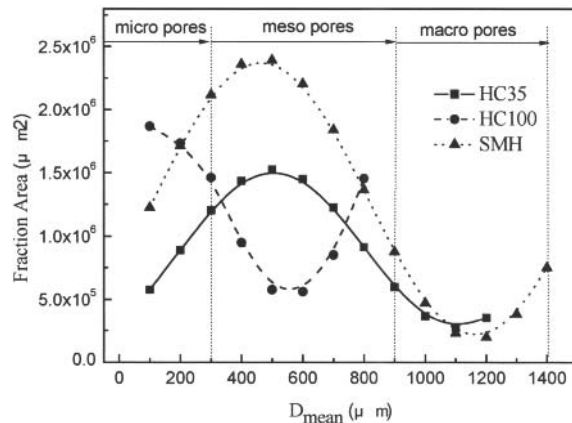

Figure 2. Pore size distribution in cathode samples

In Figure 3, the curves of pore shape distribution are plotted against the aspect ratio for the pores in the cathode samples. HC100 cathode sample has higher content of pores with aspect ratio of 1 to 3 than SMH and HC35 samples.

In general, HC35 contains more meso pores than HC100, while SMH has the majority of pores in the meso pores range. HC100 is mainly composed of the micropores with smaller total porosity than HC35. Both HC35 and SMH have evenly distributed pores with a higher total porosity. For the pore shape distribution, the majority of measured pores have an aspect ratio of 1 – 3 for the all tested cathode samples.
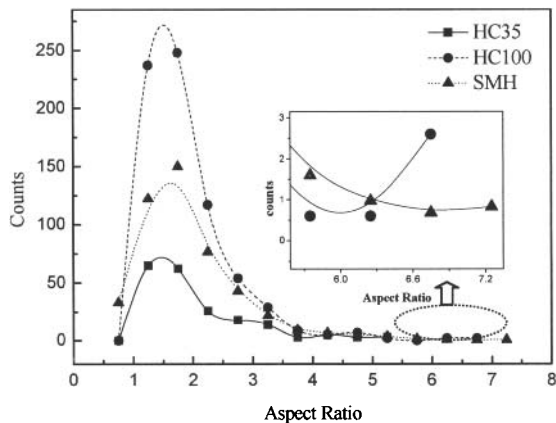

Figure 3. Pore shape distribution in cathode samples

Pores Orientation and Connectivity

Figure 4 shows the pore orientation of 180 degrees in the inner areas of the cathode samples, in which the reference direction (blue line) is perpendicular to the axis on the cross-section of the sample. In the skeleton of binary pore images, as shown in Figure 5, connected or intersected lines on the 2D segment area are used to represent the connected pores passing that area. These have been used to describe the connectivity of the pores within the cathode samples.
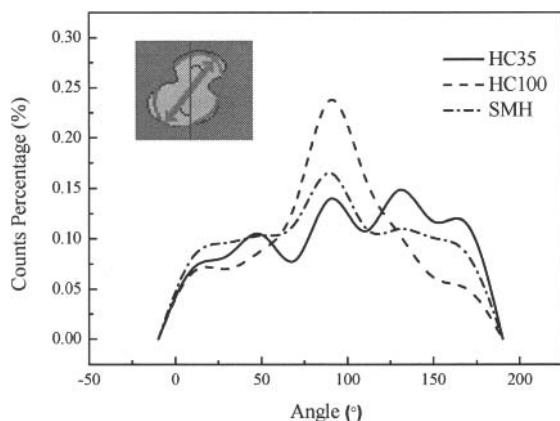

Figure 4. Orientation of pores in cathode samples (The upper-left sketch illustrates the orientation of a pore)

It was individually observed that part of the pores in the HC35 cathode was aligned in certain directions, roughly showing a higher connectivity. HC100 sample exhibited numerous micropores randomly distributed but a certain orientation massively connected through the cross-section of the sample. However, the pores in SMH cathode samples were evenly distributed and the connection among these pores was also randomly orientated.
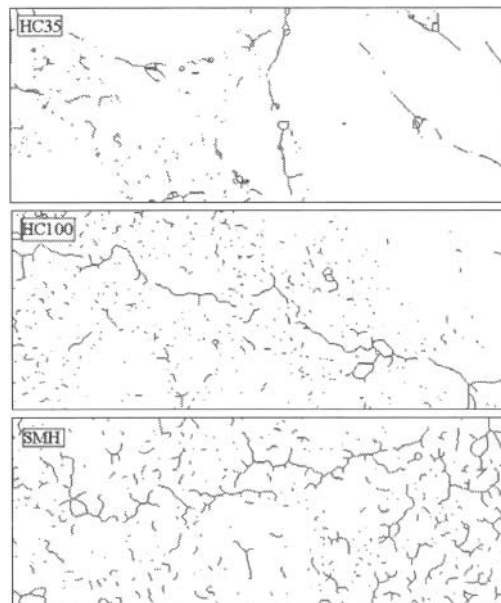

Figure 5. Skeletonization of pore images for cathode samples

Sodium and Fluoride Penetration

Figure 6 shows the extent of sodium and fluoride penetration within the cathode samples after aluminum electrolysis. Figure 7 shows the micrographs of the cross-sections of HC35, HC100 and SMH, where the porous structures within these carbon cathodes can also facilitate this penetration.
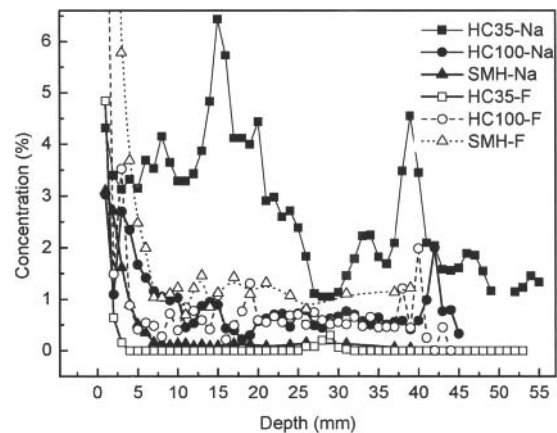

Figure 6. Penetrated sodium and fluoride vs. the penetration depth in cathode samples after aluminum electrolysis (960 C, 3 hr)

1105

The sodium generation during aluminum electrolysis can be expressed by the reactions below:

$$Al(l) + 3NaF(l) = 3Na(in\ C) + AlF_3(l) \qquad (2)$$

$$Na(in\ Al) \rightarrow Na(in\ C) \qquad (3)$$

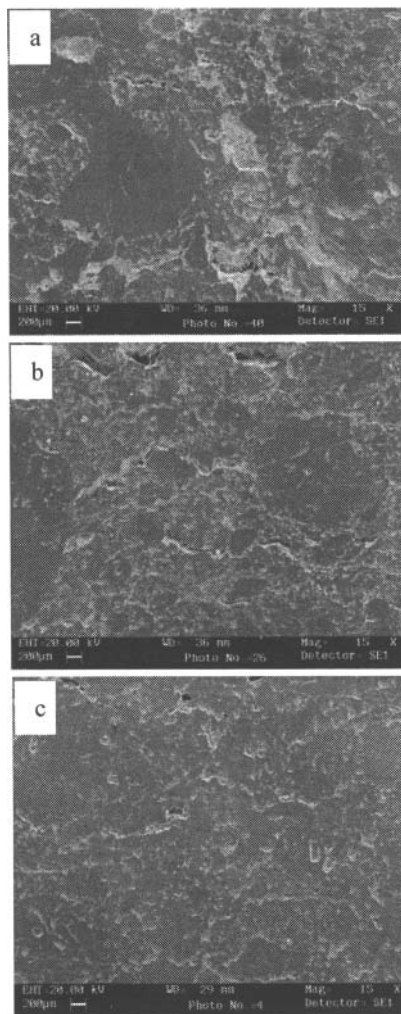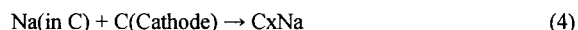$$Na(in\ C) + C(Cathode) \rightarrow C_xNa \qquad (4)$$

Figure 7. SEM micrographs of the cross-sections of cathode samples: a) HC35, b) HC100, and c) SMH

The sodium can continuously migrate into the whole areas within the carbon cathodes. It can be seen that the percentage of penetrated sodium, which could include both metallic Na and NaF or Na_3AlF_6, increases in the order of HC35 > HC100 > SMH, which is similar to their order in the degree of graphitization. This means that the fully graphitized cathode material, SMH, has the best resistance to the sodium attack, which is in agreement with the sodium expansion results in previous Rapoport tests [13,14]. Here the sodium penetration is found less sensitive to the porosity variation of the various cathode materials investigated, and in fact the graphitized cathode sample has higher porosity than the full graphitic one.

However, fluoride penetration is more dependent on the porous structures of the cathode samples. The percentage of penetrated fluorine increases in the order of SMH > HC100 > HC35, which is similar to their order in the open porosity (see Table I) and the partial porosity of micropores (see Table II). The micropores may play an important role in providing inner channels and capillary force for the bath penetration during aluminum electrolysis. Within the inner area of the carbon cathodes, the penetrated fluorine containing compounds might take more complex chemical forms, for instance, in NaF, AlF_3, Na_3AlF_6 and CaF_2.

In addition, the strong fluctuation of penetrated sodium against the penetration depth within the HC35 sample could be due to the uneven pore connectivity and pore orientation (see Figure 4), as well as a fluctuating pathway caused by mixture of coke and anthracite grains in the sample inner area.

It is primarily important in this work that some pore parameters, such as pore orientation and connectivity, pore size and shape distribution, etc, have been identified for their possible relevance to the sodium and fluoride penetration and cathode performance. The method is still under development, and more carbon cathode samples will be collected for systematical investigation.

Conclusions

1. Carbon and graphite cathode materials can be characterized using an image analysis method for the porosity, total number of pores, pore size and shape distribution, pore orientation and connectivity. The results can be combined with SEM-EDS analysis to evaluate sodium and fluoride penetration into the carbons.

2. Graphitized cathode material has high total porosity but even pore size distribution, while it shows a strong resistance to sodium penetration in aluminum electrolysis.

3. Full graphitic cathode material has higher total porosity and higher partial porosity in micropores than the semi-graphitic cathode materials, showing better resistance to the sodium penetration but higher fluoride penetration.

4. Semi-graphitic cathode material has higher open porosity while lower partial porosity in micropores than the full graphitic and graphitized cathode materials, exhibiting poor resistance to sodium penetration but low fluoride penetration.

References

1. Morten Sørlie and Harald A. Øye, *Cathodes in Aluminum Electrolysis* (Dusseldorf, FRG: Aluminium-Verlag GmbH, 1994), 282-361..

2. P. Clery, "Green Paste Density as an Indicator of Mixing Efficiency," *Light metals 1998*, ed. B. J. Welch (Warendale, PA: The Minerals, Metals & Materials Society, 1998), 625-626.

3. J. Xue, H. A. Øye, "Investigating Carbon/ TiB_2 Materials for Aluminum Reduction Cathodes," *JOM*, 1992, 44(11): 28~34

4. P.Y. Brisson, G. Soucy, M. Fafard. "Revisiting Sodium and Bath Penetration in the Carbon Lining of Aluminum Electrolysis cell," *Light Metals 2005*, ed. H. Kvande (Warendale, PA: The Minerals, Metals & Materials Society, 2005), 727~732.

5. J. L. Eilertsen et al., "An Automatic Image Analysis of Coke Texture," *Carbon*, 34 (3) (1996), 375-385.

6. M. Tkac, T. Foosnaes and H. A. Øye, "Effect of Vacuum Vibro-forming on Porosity Development during Anode Baking," *Light metals 2007*, ed. M. Sørlie (Warendale, PA: The Minerals, Metals & Materials Society, 2007), 885-890.

7. S. Rørvik and H. A. Øye, "A Method for Characterization of Anode Pore Structure by Image Analysis," *Light Metals 1996*, ed. W. Hale (Warendale, PA: The Minerals, Metals & Materials Society, 1996), 561-568.

8. A. N. Adams. "The Use of Image Analysis for the Optimization of Pre-Baked Anode Formulation," *Light metals 2002*, ed. W. A. Schneider (Warendale, PA: The Minerals, Metals & Materials Society, 2002), 547-552.

9. S. Rørvik, A. P. Ratvik and T. Foosnaes, "Characterization of Green Anode Materials by Image Analysis," *Light Metals 2006*, ed. J. G. Travis (Warendale, PA: The Minerals, Metals & Materials Society, 2006), 553-558.

10. ASTM D2797-85 Standard Practice for Preparing Coal Samples for Microscopical Analysis by Reflected Light. ASTM International, 1999.

11. J. Xue, Q. Liu, and J. Zhu, "Sodium Penetration into Carbon-Based Cathodes during Aluminum Electrolysis," *Light Metals 2006*, ed. J. G. Travis (Warendale, PA: The Minerals, Metals & Materials Society, 2006), 651-654.

12. S. A. Saltykov, *Stereometric Metallography* (Moscow, State Publishing House for Metals and Sciences, 1958), 3nd ed., 1970

13. J. Xue, et al, "Characterization of Sodium Expansion in Industrial Graphitic and Graphitized Cathodes", *Light Metals 2010*, ed. J. A. Johnson (Warendale, PA: The Minerals, Metals & Materials Society, 2006), 651-654.

14. J. G. Hop, "Sodium Expansion and Creep of Cathode Carbon," (Dr.ing Thesis, Norwegian University of Science and Technology, 2003), 179.